

Numerical Comparison of Leja and Clenshaw-Curtis Dimension-Adaptive Collocation for Stochastic Parametric Electromagnetic Field Problems

Dimitrios Loukrezis^{1,2}, Ulrich Römer³, and Herbert De Gersem^{1,2}

¹Institut für Theorie Elektromagnetischer Felder, Technische Universität Darmstadt,
Schlossgartenstraße 8, 64289 Darmstadt, Germany

²Graduate School for Computational Engineering, Technische Universität Darmstadt,
Dolivostraße 15, 64293 Darmstadt, Germany

³Institut für Dynamik und Schwingungen, Technische Universität Braunschweig,
Schleinitzstraße 20, 38106 Braunschweig, Germany

Abstract

We consider the problem of approximating the output of a parametric electromagnetic field model in the presence of a large number of uncertain input parameters. Given a sufficiently smooth output with respect to the input parameters, such problems are often tackled with interpolation-based approaches, such as the stochastic collocation method on tensor-product or isotropic sparse grids. Due to the so-called curse of dimensionality, those approaches result in increased or even forbidding computational costs. In order to reduce the growth in complexity with the number of dimensions, we employ a dimension-adaptive, hierarchical interpolation scheme, based on nested univariate interpolation nodes. Clenshaw-Curtis and Leja nodes satisfy the nestedness property and have been found to provide accurate interpolations when the parameters follow uniform distributions. The dimension-adaptive algorithm constructs the approximation based on the observation that not all parameters or interactions among them are equally important regarding their impact on the model's output. Our goal is to exploit this anisotropy in order to construct accurate polynomial surrogate models at a reduced computational cost compared to isotropic sparse grids. We apply the stochastic collocation method to two electromagnetic field models with medium- to high-dimensional input uncertainty. The performances of isotropic and adaptively constructed, anisotropic sparse grids based on both Clenshaw-Curtis and Leja interpolation nodes are examined. All considered approaches are compared with one another regarding the surrogate models' approximation accuracies using a cross-validation error metric.

keywords— dimension adaptivity, Clenshaw-Curtis, computational electromagnetics, electromagnetic field simulations, hierarchical interpolation, Leja, sparse grids, stochastic collocation, uncertainty quantification.

1 Introduction

More often than ever before, the design phase of electric and electronic devices, e.g. electric machines or high-frequency (HF) components, incorporates parameter studies in order to predict the device's

behavior under uncertainty. This uncertainty, e.g. with respect to the device’s geometry, materials or other, often stems from tolerances during the manufacturing process. As part of those uncertainty quantification (UQ) studies, one typically investigates a specific output of the device, called the quantity of interest (QoI), and tries to estimate statistical moments or sensitivities, with the goal of reducing the risk of malfunction, misfire or other type of failure. Another common goal is the construction of a sufficiently accurate surrogate model, which could serve as a computationally inexpensive substitute to the original model. This latter goal will be the focus of the present paper.

Given a QoI which depends smoothly on a set of input parameters, UQ problems can be efficiently resolved with the use of polynomial approximations. Most commonly, stochastic Galerkin [2, 12, 22], stochastic collocation [1, 3, 6, 35] or point collocation [5, 24, 25] methods are employed. The stochastic Galerkin method is often labeled as “intrusive”, due to the fact that dedicated solvers have to be developed in order to tackle the stochastic problem at hand. The additional programming effort is usually regarded as a major disadvantage, especially in the case of complex computational models whose software and underlying solvers are difficult to be accessed, modified or otherwise manipulated. Therefore, and despite the fact that stochastic Galerkin methods have nice properties for error analysis and estimation, collocation methods are generally preferred in this context, as they allow for a non-intrusive, black-box use of the original computational models. It must be noted that the separation of methods into intrusive and non-intrusive is an ongoing topic of discussion, see e.g. [13]. In the context of the present paper we shall retain the usual distinction. Comparisons between stochastic and point collocation methods, see e.g. [9], indicate that the former tends to provide superior accuracies and convergence rates. However, since these approaches differ significantly, a fair comparison between the two is still an open research topic, as also indicated in [24].

A common bottleneck of all aforementioned methods is the so-called “curse of dimensionality” [4], i.e. convergence rates deteriorate and computational costs increase with the number of considered input parameters, often exponentially. As a possible remedy, state-of-the-art methods employ sparse, adaptively constructed polynomial approximations, see e.g. [7, 26, 29, 32] for adaptive stochastic collocation methods and [5, 23] for adaptive point collocation methods. In the case of adaptive stochastic collocation methods, sparse approximations are based on nested interpolation nodes. When the parameters follow uniform distributions, a typical choice is Clenshaw-Curtis nodes [29, 32]. More recently, Leja interpolation nodes have been proposed as a possible alternative [7, 26]. While generally not free of the curse of dimensionality, adaptive methods exploit possible anisotropies among the input parameters and their interactions regarding their impact upon the QoI. Assuming that such anisotropies exist, adaptive approximations may enable studies with a comparably large number of input parameters. Besides adaptive approximations, alternative methods aiming to tackle the curse of dimensionality are also available, e.g. tensor decompositions (see [15] and the references therein) or active subspaces (see [8] and the references therein).

In the present paper, we consider medium- to high-dimensional UQ electromagnetic field (EMF) problems. Our goal is to construct surrogate models which could reliably replace the original ones in computationally demanding tasks, e.g. failure probability estimations or robust optimization. Therefore, the surrogate model’s accuracy is a critical factor. For that purpose, we investigate the application of the sparse grids stochastic collocation method in the context of EMF simulations. Specifically, we compare isotropic and adaptive, anisotropic sparse collocation schemes employing Clenshaw-Curtis and Leja interpolation nodes with respect to accuracy and computational work. Isotropic sparse grids are constructed with Smolyak’s formula [33]. The adaptive construction of sparse grids is based on a dimension-adaptive algorithm, similar to the ones presented in [11] for adaptive quadrature and in [20] for adaptive interpolation. In the search of an acceptable compromise between computational work and approximation accuracy, adaptivity is a topic which is receiving increasing attention in uncertainty quantification. In the same context, the choice of collocation

nodes employed in adaptive schemes remains an active field of research. However, comparisons of different strategies have rarely been addressed. Available literature is scarce and so far considers problems in a purely mathematical context, e.g. approximations of multivariate functions or parametric elliptic partial differential equations [7, 26, 27]. To our knowledge, such comparisons have not been performed in the context of concrete engineering applications, such as EMF models and simulations. Similarly, Leja nodes remain practically unknown as an option for UQ or other parametric problems in complex engineering applications.

The rest of the paper is organized as follows. In Section 2 we offer a general description of the approximation problem at hand. In Section 3 we present the approximation method of choice, i.e. the interpolation-based stochastic collocation method on sparse grids. Univariate and tensor-product collocation, which are used as “building blocks” for sparse grids collocation, are presented in Sections 3.1 and 3.2, respectively. The construction of isotropic and adaptive, anisotropic sparse grids is presented in Sections 3.3.1 and 3.3.2, respectively. Section 4 presents the EMF applications and the respective numerical results. All considered collocation methods are first tested on an academic benchmark example in Section 4.1. A real-world application is presented in Section 4.2.

2 Problem Setting

Let (Θ, Σ, P) be a probability space, $\theta \in \Theta$ a random event and $\mathbf{Y} = (Y_1, Y_2, \dots, Y_N)$ a vector of N independent random variables (RVs) defined on (Θ, Σ, P) . We denote with $\mathbf{y} = \mathbf{Y}(\theta)$ a random realization of the input RVs and with $\varrho_{\mathbf{Y}}$ their joint probability density function (PDF), such that $\mathbf{Y} : \Theta \rightarrow \Gamma \subset \mathbb{R}^N$ and $\varrho_{\mathbf{Y}} : \Gamma \rightarrow \mathbb{R}_+$. In the context of the present work, Γ is an N -dimensional hyper-rectangle $\Gamma = \Gamma_1 \times \Gamma_2 \times \dots \times \Gamma_N$. A uniform univariate PDF $\varrho_n(y_n)$ corresponds to each Γ_n , $n = 1, 2, \dots, N$. Due to the statistical independence of the RVs, the joint PDF is given by

$$\varrho_{\mathbf{Y}}(\mathbf{y}) = \prod_{n=1}^N \varrho_n(y_n). \quad (1)$$

We are interested in approximating an output of a computational model which depends on the RVs \mathbf{Y} . This output is typically referred to as the quantity of interest (QoI) and is here denoted with q . Preferably, the dependence of the QoI on the input RVs is smooth, ideally analytic. We seek an approximation in the form of a polynomial surrogate model, such that

$$q(\mathbf{y}) \approx \tilde{q}(\mathbf{y}) = \sum_i s_i \Psi_i(\mathbf{y}), \quad (2)$$

where Ψ_i are multivariate polynomials and s_i are real or complex coefficients. Multivariate polynomials Ψ_i can be conveniently chosen as tensor-product polynomials

$$\Psi_i(\mathbf{y}) = \prod_{n=1}^N \psi_{i_n}(y_n), \quad (3)$$

where ψ_{i_n} refers to a univariate polynomial in dimension n . Each combination of local indices i_1, \dots, i_N in (3) is uniquely associated to a global index i .

We aim at reducing the error of the surrogate model uniformly in Γ , which is relevant in the context of failure probabilities. We assume that the model which provides the considered QoI is complex, in the sense that its software and underlying solvers are difficult to be accessed and modified. Therefore, we rely on non-intrusive methods, which use the original computational model in

a black-box fashion, i.e. without any modifications. Moreover, we assume that the computational cost of one call to the original computational model, e.g. in order to compute the QoI for a given set of parameter values, is significantly higher than all other numerical operations during the surrogate model's construction. Therefore, the total cost of the approximation can be predominantly attributed to the required number of original model evaluations, i.e. calls to the original model. Consequently, we are interested in minimizing the number of model evaluations while still achieving desired accuracies.

3 Sparse Grids Stochastic Collocation

Using the stochastic collocation method, the polynomial approximation (2) is constructed by interpolating specific values of the QoI. Those values are provided by evaluating the QoI on a set of realizations of the input RVs, called collocation points. We denote the set of collocation points with $\Xi = \{\mathbf{y}^{(i)}\}$ and its cardinality with $\#\Xi$. The choice of collocation points depends on the PDF $\varrho_{\mathbf{Y}}$ which characterizes the input RVs. Lagrange polynomials are typically employed for the interpolation. Since the QoI has to be evaluated on all collocation points and because each evaluation requires a call to the original deterministic model, the computational cost of the method depends predominantly on $\#\Xi$.

3.1 Univariate collocation

Univariate interpolation rules are used as building blocks for stochastic collocation in multiple dimensions, respectively, multiple random parameters. Therefore, let us first consider the case of only one such parameter, Y_n .

We introduce the non-negative integer $\ell_n \in \mathbb{N}_0$, called the interpolation level. The corresponding univariate grid of interpolation nodes, respectively, collocation points, is denoted with Ξ_{ℓ_n} . The number of univariate collocation points $\#\Xi_{\ell_n}$ is associated with the level ℓ_n through a monotonically increasing "level-to-nodes" function $m_n : \mathbb{N}_0 \rightarrow \mathbb{N}$, such that $\#\Xi_{\ell_n} = m_n(\ell_n)$. The choice of collocation points depends on the PDF ϱ_n . In the case of uniform distributions, common choices are Gauss-Legendre, Clenshaw-Curtis or Leja interpolation nodes. Gauss-Legendre nodes correspond to zeros of Legendre polynomials, Clenshaw-Curtis nodes to extrema of Chebyshev polynomials and Leja nodes are sequences of points such that

$$y^{(K)} = \arg \max_{y \in [a, b]} \prod_{k=0}^{K-1} |y - y^{(k)}|, \quad (4)$$

where a and b are the limits of the corresponding uniform distribution.

Given a set of univariate collocation points $\Xi_{\ell_n} = \{y_n^{(i_n)}\}_{i_n=1}^{m_n(\ell_n)}$, the nodal Lagrange basis polynomials of degree $m_n(\ell_n) - 1$ are defined as

$$l_{i_n}^{\ell_n}(y_n) = \prod_{k=1, k \neq i_n}^{m_n(\ell_n)} \frac{y_n - y_n^{(k)}}{y_n^{(i_n)} - y_n^{(k)}}, \quad (5)$$

$$l_1^0(y_n) = 1.$$

Assuming now that the QoI depends only on RV Y_n and denoting the univariate Lagrange operator with \mathcal{I}_{ℓ_n} , the interpolation formula reads

$$\mathcal{I}_{\ell_n} q(y_n) = \sum_{i_n=1}^{m_n(\ell_n)} q(y_n^{(i_n)}) l_{i_n}^{\ell_n}(y_n). \quad (6)$$

3.2 Tensor-product collocation

In its simplest form, multivariate collocation consists of tensor-product combinations of univariate interpolation grids and operators. We introduce the multi-index $\boldsymbol{\ell} = (\ell_1, \ell_2, \dots, \ell_N) \in \mathbb{N}_0^N$, which contains the interpolation level for each RV. Generally, indices $\ell_1, \ell_2, \dots, \ell_N$ can have different values from one another. The special case where $\ell_n = \ell, \forall n = 1, 2, \dots, N$, is called “isotropic” tensor-product collocation.

The multivariate collocation points are given as the tensor grid

$$\begin{aligned} \Xi_{\boldsymbol{\ell}} &= \Xi_{\ell_1} \times \Xi_{\ell_2} \times \dots \times \Xi_{\ell_N} \\ &= \left\{ y_1^{(i_1)} \right\}_{i_1=1}^{m_1(\ell_1)} \times \left\{ y_2^{(i_2)} \right\}_{i_2=1}^{m_2(\ell_2)} \times \dots \times \left\{ y_N^{(i_N)} \right\}_{i_N=1}^{m_N(\ell_N)}, \end{aligned} \quad (7)$$

with cardinality $\#\Xi_{\boldsymbol{\ell}} = \#\Xi_1 \# \Xi_2 \dots \# \Xi_N$. Every multivariate collocation point $\mathbf{y}^{(i)} \in \Xi_{\boldsymbol{\ell}}$ is uniquely defined by the multi-index $\mathbf{i} = (i_1, i_2, \dots, i_N)$, such that $\mathbf{y}^{(i)} = (y_1^{(i_1)}, y_2^{(i_2)}, \dots, y_N^{(i_N)})$. The corresponding multivariate nodal Lagrange polynomials, $L_{\mathbf{i}}^{\boldsymbol{\ell}}$ are defined as

$$L_{\mathbf{i}}^{\boldsymbol{\ell}}(\mathbf{y}) = \prod_{n=1}^N l_{i_n}^{\ell_n}(y_n). \quad (8)$$

Denoting the multivariate Lagrange operator corresponding to multi-index $\boldsymbol{\ell}$ with $\mathcal{I}_{\boldsymbol{\ell}}$, the interpolation formula reads

$$\begin{aligned} \mathcal{I}_{\boldsymbol{\ell}}[q](\mathbf{y}) &= (\mathcal{I}_{\ell_1} \otimes \mathcal{I}_{\ell_2} \otimes \dots \otimes \mathcal{I}_{\ell_N}) q(\mathbf{y}) \\ &= \sum_{i_1=1}^{m_1(\ell_1)} \sum_{i_2=1}^{m_2(\ell_2)} \dots \sum_{i_N=1}^{m_N(\ell_N)} q(y_1^{(i_1)}, y_2^{(i_2)}, \dots, y_N^{(i_N)}) \prod_{n=1}^N l_{i_n}^{\ell_n}(y_n) \\ &= \sum_{\mathbf{i}: \mathbf{y}^{(i)} \in \Xi_{\boldsymbol{\ell}}} q(\mathbf{y}^{(i)}) L_{\mathbf{i}}^{\boldsymbol{\ell}}(\mathbf{y}). \end{aligned} \quad (9)$$

While simple in its conception and construction, tensor-product stochastic collocation becomes intractable for a large number N of RVs. The curse of dimensionality is particularly evident in the case of isotropic tensor grids, where $\#\Xi_{\boldsymbol{\ell}} = m(\ell)^N$, i.e. the required computational work increases exponentially with respect to N . Therefore, the use of tensor-product stochastic collocation is restricted to low-dimensional settings.

3.3 Sparse Grids Collocation

In high-dimensional settings, collocation on sparse grids is typically employed as a way to mitigate the computational cost of the full tensor-product collocation. Sparse grids are based on specific combinations of tensor-product grids, resulting in a reduced number of collocation points and, respectively, model evaluations. Depending on the grid’s construction process, we distinguish between isotropic and adaptive, anisotropic sparse grids and corresponding collocation schemes.

3.3.1 Isotropic sparse grids

We first refer to the construction of isotropic sparse grids [1, 3, 6, 28]. We define the approximation level $\ell \in \mathbb{N}_0$ and enforce the restriction

$$|\ell| = \sum_{n=1}^N \ell_n \leq \ell. \quad (10)$$

The sparse grid is then constructed as a linear combination of all tensor-product grids Ξ_ℓ , as defined in (7), whose multi-index ℓ satisfies the admissibility condition (10). Further, introducing the difference operators

$$\Delta_{\ell_n} := \mathcal{I}_{\ell_n} - \mathcal{I}_{\ell_n-1}, \quad (11)$$

$$\Delta_\ell := \Delta_{\ell_1} \otimes \Delta_{\ell_2} \otimes \cdots \otimes \Delta_{\ell_N}, \quad (12)$$

where \mathcal{I}_{-1} is the null operator, the Smolyak interpolation formula [33] reads

$$\mathcal{S}_\ell q(\mathbf{y}) = \sum_{|\ell| \leq \ell} \Delta_\ell q(\mathbf{y}) = \sum_{\ell-N+1 \leq |\ell| \leq \ell} (-1)^{\ell-|\ell|} \binom{N-1}{\ell-|\ell|} \mathcal{I}_\ell q(\mathbf{y}). \quad (13)$$

We should note that formula (13) is in general not interpolatory, except for the case of nested univariate collocation points, for which holds that $\Xi_{\ell_n-1} \subset \Xi_{\ell_n}$ [3]. The corresponding sparse grid of collocation points is given by

$$\Xi_\ell^S = \bigcup_{\ell-N+1 \leq |\ell| \leq \ell} \Xi_\ell. \quad (14)$$

While a closed-form formula for the computation of the exact number of collocation points $\#\Xi_\ell^S$ is not available, the growth complexity is $\mathcal{O}\left(m(\ell)(\log m(\ell))^{N-1}\right)$ [6], which is much milder than the $\mathcal{O}\left(m(\ell)^N\right)$ for the full tensor-product collocation. Therefore, even though isotropic sparse grids are obviously not free of the curse of dimensionality, they are usable up to a moderate number of RVs.

3.3.2 Adaptive anisotropic sparse grids

It is often the case that certain parameters or parameter combinations and interactions have a more significant impact on the QoI than others. This parameter anisotropy can be exploited by using anisotropic sparse grids [29]. In this way, the sparse grid is constructed only with those multi-indices and collocation points which add significant contributions to the approximation. Therefore, we expect to save computational effort, while obtaining similar or better accuracies. In this section, we present a greedy, dimension-adaptive strategy to achieve this goal. Our approach is based on the methods and algorithms presented in [11] for quadrature purposes and in [20] for interpolation purposes. While Leja nodes have not been considered in those works, the extension of the presented methods and algorithms to Leja nodes is straightforward. Similar dimension-adaptive approaches are suggested in [7, 26] for Leja nodes and in [17, 32] for Clenshaw-Curtis nodes.

We first re-visit the univariate collocation described in Section 3.1 and restrict the choice of interpolation nodes to nested sequences $\Xi_{\ell_n-1} \subset \Xi_{\ell_n}$. The nestedness constraint is satisfied by Clenshaw-Curtis nodes with the level-to-nodes function $m_n(\ell_n) = 2^{\ell_n} + 1$. As can be observed in (4), Leja nodes are nested by construction and the corresponding level-to-nodes function is $m_n(\ell_n) =$

$\ell_n + 1$. We should note that, while in this work we only consider uniformly distributed parameters, the ideas and algorithms are applicable to any distribution, assuming that a corresponding family of nested nodes is available. E.g., in the case of Gaussian distributions, Gauss-Kronrod-Patterson nodes satisfy the nestedness constraint [32]. Moreover, the use of Leja nodes with non-uniform probability measures, particularly the ones relative to the Wiener-Askey polynomial chaos [36], is discussed in [26].

Employing nestedness, higher order approximations can be hierarchically constructed by a step-by-step refinement of the interpolation level and re-use of the lower level approximations at each step [7, 20, 32]. Using the difference operator defined in (11) the hierarchical interpolation operator is defined as

$$\mathcal{I}_{\ell_n} = \sum_{k=0}^{\ell_n} \Delta_k. \quad (15)$$

We define the hierarchical Lagrange basis polynomials $h_{i_n}^{\ell_n}$, such that

$$h_{i_n}^{\ell_n}(y_n) = \begin{cases} l_{i_n}^{\ell_n}(y_n), & y_n^{(i_n)} \in \Xi_{\ell_n} \setminus \Xi_{\ell_n-1}, \\ h_{i_n}^{\ell_n-1}(y_n), & y_n^{(i_n)} \notin \Xi_{\ell_n} \setminus \Xi_{\ell_n-1}, \end{cases} \quad (16)$$

where $l_{i_n}^{\ell_n}$ is the nodal Lagrange basis polynomial defined in (5). Then, the hierarchical univariate Lagrange interpolation operator reads

$$\mathcal{I}_{\ell_n} q(y) = \mathcal{I}_{\ell_n-1} q(y) + \sum_{i_n : y_n^{(i_n)} \in \Xi_{\ell_n} \setminus \Xi_{\ell_n-1}} \underbrace{\left(q(y_n^{(i_n)}) - \mathcal{I}_{\ell_n-1} q(y_n^{(i_n)}) \right)}_{\text{hierarchical surplus } s_{i_n}^{\ell_n}} h_{i_n}^{\ell_n}(y). \quad (17)$$

The hierarchical surplus $s_{i_n}^{\ell_n}$ determines the contribution of the new interpolation node $y_n^{(i_n)} \in \Xi_{\ell_n} \setminus \Xi_{\ell_n-1}$ compared to the already available approximation \mathcal{I}_{ℓ_n-1} .

In the multivariate case, we assume that the multi-indices which are employed in the interpolation form the multi-index set Λ . The corresponding interpolation operator is denoted with \mathcal{I}_{Λ} and the corresponding sparse grid with Ξ_{Λ} . We enforce upon the multi-index set Λ a monotonicity constraint, such that

$$\forall \ell \in \Lambda \Rightarrow \ell - \mathbf{e}_n \in \Lambda, \forall n = 1, 2, \dots, N, \text{ with } \ell_n > 0, \quad (18)$$

where $\mathbf{e}_n = (\delta_{mn})_{1 \leq m \leq N}$ is the n -th unit vector and δ_{mn} denotes the Kronecker delta. Monotone sets are also known as downward-closed sets. Then, the multivariate interpolation is defined as

$$\mathcal{I}_{\Lambda} q(\mathbf{y}) = \sum_{\ell \in \Lambda} \Delta_{\ell}, \quad (19)$$

where the multivariate difference operators Δ_{ℓ} are defined as in (12). It must be noted that the isotropic sparse grids described in Section 3.3.1 satisfy the monotonicity constraint by construction. Assuming a multi-index $\ell \notin \Lambda$ such that the set $\Lambda \cup \ell$ is monotone, the hierarchical interpolation scheme reads

$$\mathcal{I}_{\Lambda \cup \ell} q(\mathbf{y}) = \mathcal{I}_{\Lambda} q(\mathbf{y}) + \sum_{\mathbf{i} : \mathbf{y}^{(\mathbf{i})} \in \Xi_{\Lambda \cup \ell} \setminus \Xi_{\Lambda}} \underbrace{\left(q(\mathbf{y}^{(\mathbf{i})}) - \mathcal{I}_{\Lambda} q(\mathbf{y}^{(\mathbf{i})}) \right)}_{\text{hierarchical surplus } s_{\mathbf{i}}^{\ell}} H_{\mathbf{i}}^{\ell}(\mathbf{y}), \quad (20)$$

where $H_{\mathbf{i}}^{\ell}$ are multivariate hierarchical Lagrange polynomials, defined as

$$H_{\mathbf{i}}^{\ell}(\mathbf{y}) = \prod_{n=1}^N h_{i_n}^{\ell_n}(y_n). \quad (21)$$

Data: QoI q , number of RVs N , monotone multi-index set Λ , tolerance ϵ , budget B

Result: sparse grid $\Xi_{\Lambda \cup \mathcal{A}(\Lambda)}$, approximation $\mathcal{I}_{\Lambda \cup \mathcal{A}(\Lambda)}$

repeat

$\ell_{\text{new}} = \arg \max_{\ell \in \mathcal{A}(\Lambda)} \eta_{\ell}$
 update Λ and \mathcal{I}_{Λ} as in (20)
 update $\mathcal{A}(\Lambda)$ as in (23)
 compute s_i^{ℓ} , $\forall \ell \in \mathcal{A}(\Lambda)$ as in (20)
 compute η_{ℓ} , $\forall \ell \in \mathcal{A}(\Lambda)$ as in (24)

until $\text{termination}[\mathcal{A}(\Lambda), \epsilon, B]$;

Algorithm 1: Dimension-adaptive collocation algorithm

Regarding the adaptive refinement of the polynomial approximation and the construction of the corresponding sparse grid, i.e. the choice of the multi-index ℓ to be added to set Λ in (20), several approaches are available in literature, see e.g. [7, 11, 14, 17, 26, 27, 29, 32]. A short description of the dimension-adaptive algorithm employed in the context of this work is provided in Algorithm 1. A general overview of the approach follows.

We assume that a monotone multi-index set Λ is available. All possible refinements of the multi-indices comprising set Λ form the refinement set

$$\mathcal{R}(\Lambda) = \{\ell + \mathbf{e}_n, \forall \ell \in \Lambda, \forall n = 1, 2, \dots, N\}. \quad (22)$$

The admissible multi-indices to be added to set Λ form the admissible set

$$\mathcal{A}(\Lambda) = \{\ell \in \mathcal{R}(\Lambda) : \ell \notin \Lambda \text{ and } \Lambda \cup \ell \text{ is monotone}\}. \quad (23)$$

We note that, when an approximation and its corresponding monotone multi-index set are not already available, Algorithm 1 is initialized with $\Lambda = \{(0, 0, \dots, 0)\}$. Each one of the admissible indices in $\mathcal{A}(\Lambda)$ defines a set of collocation points to be possibly added to Ξ_{Λ} . Using (20), we compute the hierarchical surpluses which correspond to the new collocation points. The dimension-adaptivity is based on error indicators η_{ℓ} , $\ell \in \mathcal{A}(\Lambda)$, computed after the corresponding hierarchical surpluses. In the context of the present work, error indicators are given by

$$\eta_{\ell} = \frac{1}{\#(\Xi_{\Lambda \cup \ell} \setminus \Xi_{\Lambda})} \sum_{\substack{\mathbf{i}: \mathbf{y}^{(i)} \in \Xi_{\Lambda \cup \ell} \setminus \Xi_{\Lambda} \\ \ell \in \mathcal{A}(\Lambda)}} |s_i^{\ell}|, \quad (24)$$

as proposed in [11]. Other suggestions on computing local error indicators can be found in [17, 26, 32]. The admissible multi-index to be added to Λ is the one with the maximum contribution compared to the already available approximation, i.e. the one corresponding to the maximum η_{ℓ} . The algorithm terminates either when a pre-defined simulation budget B , i.e. number of model evaluations, is reached or when the total contribution of set $\mathcal{A}(\Lambda)$ is below a specified tolerance ϵ [11, 17, 26, 20, 32]. The termination conditions can be formally formulated as

$$\# \Xi_{\Lambda \cup \mathcal{A}(\Lambda)} \geq B, \quad (25a)$$

$$\sum_{\ell \in \mathcal{A}(\Lambda)} \eta_{\ell} \leq \epsilon. \quad (25b)$$

Since the hierarchical surpluses and collocation points for the admissible multi-indices are already available, the sparse grid and the corresponding approximation after the algorithm's termination is constructed with all multi-indices in the set $\Lambda \cup \mathcal{A}(\Lambda)$.

4 Numerical Experiments

We test four variants of the sparse grids stochastic collocation method, namely isotropic and adaptive, anisotropic sparse grids collocation based on Clenshaw-Curtis and Leja interpolation nodes. In the presented results, “CC” and “LJ” refer to Clenshaw-Curtis and Leja nodes, respectively. Accordingly, subscript “iso” refers to isotropic sparse grids and subscript “adapt” to anisotropic, adaptively constructed grids. The Sparse Grids MATLAB Kit [34] has been employed for the implementation of isotropic sparse grids. Results of the Clenshaw-Curtis isotropic sparse grids have been validated with the Sparse Grids Interpolation Toolbox [19, 20], which has also been used for implementing the Clenshaw-Curtis adaptive collocation. We note that the authors of [19, 20] use the term “Clenshaw-Curtis” for nodes given by the Newton-Cotes rule and the term “Chebyshev” for the extrema of Chebyshev polynomials which are typically known as Clenshaw-Curtis nodes. Therefore, the “Chebyshev” option should be used in the toolbox. An in-house, Python-based implementation has been developed for the adaptive Leja collocation. As part of our implementation, univariate Leja nodes are computed with the Python package Chaospy [10]. All collocation variants are applied to two EMF applications, namely a dielectric slab waveguide and a Stern-Gerlach magnet. Both computational models employ in-house developed MATLAB/Octave and Python softwares. The accuracy of the surrogate models is measured with a cross-validation error metric. Using a validation set with M random realizations of the input parameters, the cross-validation error ϵ_{cv} is computed as

$$\epsilon_{cv} = \max_{m=1,2,\dots,M} \left| \tilde{q}(\mathbf{y}^{(m)}) - q(\mathbf{y}^{(m)}) \right|, \quad (26)$$

where \tilde{q} and q denote the surrogate and the original model, respectively.

4.1 Dielectric Slab Waveguide

We consider an academic example from the field of high-frequency computational electromagnetics. In particular, we consider a three-dimensional, rectangular, dielectric slab waveguide, as the one illustrated in Fig. 1. Such structures provide us with simple models, typically used to study wave-confinement mechanisms. The waveguide operates in the frequency range $[f_{\min}, f_{\max}]$. We consider uncertainties with respect to the waveguide’s geometry and material parameters. We shall construct approximations with respect to the waveguide’s reflection coefficient, also known as the S_{11} parameter, which quantifies the reflection of the incoming wave at port 1 of the waveguide. For this simple model, an analytical solution for S_{11} exists and is used in this first example in order to avoid the consideration of discretization errors.

4.1.1 Model

As can be seen in Fig. 1, the waveguide is filled with vacuum (blue area) and has a dielectric material in its middle (yellow area). Its geometry is defined by its width w along the x -axis, its height h along the y -axis and the vacuum offset d and dielectric filling length l along the z -axis. The red planes denote the waveguide’s input and output ports, respectively port 1 and 2. With the exception of the ports, the walls of the waveguide are considered to be perfect electrical conductors (PEC). Using

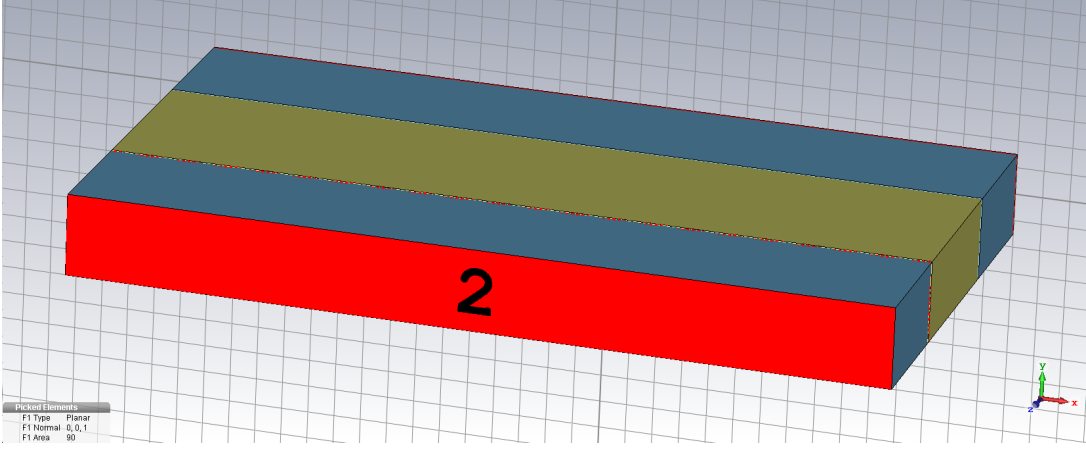


Figure 1: 3D waveguide model with dielectric filling. The yellow area denotes the dielectric filling and the blue area the vacuum. The red planes denote the waveguide ports.

the Cartesian coordinate system, the waveguide's computational domain is formally defined as

$$\Omega = [0, w] \times [0, h] \times [0, 2d + l], \quad (27a)$$

$$\Gamma_{\text{PEC}} = \{(x, y, z) \in \partial\Omega : z \neq 0 \wedge z \neq 2d + l\}, \quad (27b)$$

$$\Gamma_{\text{in}} = \{(x, y, z) \in \partial\Omega : z = 0\}, \quad (27c)$$

$$\Gamma_{\text{out}} = \{(x, y, z) \in \partial\Omega : z = 2d + l\}, \quad (27d)$$

such that $\partial\Omega = \Gamma_{\text{PEC}} \cup \Gamma_{\text{in}} \cup \Gamma_{\text{out}}$. Maxwell's source problem for the electric field \mathbf{E} reads

$$\text{curl}(\mu^{-1} \text{curl} \mathbf{E}) - \omega^2 \varepsilon \mathbf{E} = 0, \quad \text{in } \Omega, \quad (28a)$$

$$\mathbf{E} \times \mathbf{n} = 0, \quad \text{on } \Gamma_{\text{PEC}}, \quad (28b)$$

$$\mathbf{n} \times \text{curl} \mathbf{E} + \gamma \mathbf{n} \times (\mathbf{n} \times \mathbf{E}) = \mathbf{U}^{\text{inc}}, \quad \text{on } \Gamma_{\text{in}}, \quad (28c)$$

$$\mathbf{n} \times \text{curl} \mathbf{E} + \gamma \mathbf{n} \times (\mathbf{n} \times \mathbf{E}) = 0, \quad \text{on } \Gamma_{\text{out}}, \quad (28d)$$

where $\gamma = jk^{\text{inc}}$ and k^{inc} refer to the wavenumber of the incoming wave represented by \mathbf{U}^{inc} . See [18] for details. A Debye relaxation model is used for the description of the dielectric material's behavior, such that the material's electric permittivity ε and magnetic permeability μ depend on the waveguide's angular frequency ω as follows:

$$\varepsilon = \varepsilon_0 \left(\varepsilon_\infty + \sum_{k=1}^K \frac{\varepsilon_{s,k} - \varepsilon_\infty}{1 + j\omega\tau_{\varepsilon,k}} \right), \quad (29a)$$

$$\mu = \mu_0 \left(\mu_\infty + \sum_{k=1}^K \frac{\mu_{s,k} - \mu_\infty}{1 + j\omega\tau_{\mu,k}} \right). \quad (29b)$$

In (29), K denotes the relaxation model's order, index 0 refers to the material properties in vacuum, index ∞ to high frequencies and index s to the static case. For both material properties, τ denotes the characteristic relaxation time of the medium. We assume that the incoming field coincides with

Table 1: Nominal values of the waveguide's geometrical, material and source parameters.

Parameter	Symbol	Value, Model 1	Value, Model 2	Units
operating frequency	f	18-22	18-22	[GHz]
width	w	30	30	[mm]
height	h	3	3	[mm]
filling length	l	7	7	[mm]
vacuum offset	d	5	5	[mm]
vacuum permittivity	ε_0	$8.85 \cdot 10^{-12}$	$8.85 \cdot 10^{-12}$	[F/m]
high-frequency permittivity	ε_∞	1	1	[F/m]
static permittivity 1	$\varepsilon_{s,1}$	2	2	[F/m]
static permittivity 2	$\varepsilon_{s,2}$	-	2.2	[F/m]
vacuum permeability	μ_0	$4\pi \cdot 10^{-7}$	$4\pi \cdot 10^{-7}$	[H/m]
high-frequency permeability	μ_∞	1	1	[H/m]
static permeability 1	$\mu_{s,1}$	2.4	2	[H/m]
static permeability 2	$\mu_{s,2}$	-	3	[H/m]
permittivity relaxation time 1	$\tau_{\varepsilon,1}$	$1/(40\pi)$	$1/(40\pi)$	[ns]
permittivity relaxation time 2	$\tau_{\varepsilon,2}$	-	$1.1/(40\pi)$	[ns]
permeability relaxation time 1	$\tau_{\mu,1}$	$1.1/(40\pi)$	$1/(40\pi)$	[ns]
permeability relaxation time 2	$\tau_{\mu,2}$	-	$2/(40\pi)$	[ns]

the fundamental TE₁₀ mode \mathbf{e}_{10} and that higher order modes are quickly attenuated in the structure. In this case, the reflection coefficient at port 1 is an important output quantity, given as

$$q = S_{11} = C^{\text{inc}} \int_{\Gamma_{\text{in}}} \mathbf{E} \cdot \mathbf{e}_{10} \, dx, \quad (30)$$

where C^{inc} is a normalization constant.

In the most general case, we may consider uncertainties with respect to geometry, material or source parameters. Then, the parametric counterpart of (28) reads

$$\text{curl} \left(\mu(\mathbf{y})^{-1} \text{curl} \mathbf{E} \right) - \omega(\mathbf{y})^2 \varepsilon(\mathbf{y}) \mathbf{E} = 0, \quad \text{in } \Omega(\mathbf{y}), \quad (31a)$$

$$\mathbf{E} \times \mathbf{n} = 0, \quad \text{on } \Gamma_{\text{PEC}}(\mathbf{y}), \quad (31b)$$

$$\mathbf{n} \times \text{curl} \mathbf{E} + \gamma \mathbf{n} \times (\mathbf{n} \times \mathbf{E}) = \mathbf{U}^{\text{inc}}(\mathbf{y}), \quad \text{on } \Gamma_{\text{in}}(\mathbf{y}), \quad (31c)$$

$$\mathbf{n} \times \text{curl} \mathbf{E} + \gamma \mathbf{n} \times (\mathbf{n} \times \mathbf{E}) = 0, \quad \text{on } \Gamma_{\text{out}}(\mathbf{y}), \quad (31d)$$

$\rho_{\mathbf{Y}}$ -almost everywhere in Γ . A common approach in uncertainty quantification with random geometries is to pull-back the parametric equations to a fixed reference domain. This ensures the tensor-product structure of the solution space. Here, we do not approximate the solution itself, but only a scalar quantity of interest and hence, this transformation is not required. The parametric quantity of interest is given as

$$q(\mathbf{y}) = C^{\text{inc}} \int_{\Gamma_{\text{in}}(\mathbf{y})} \mathbf{E}(\mathbf{y}) \cdot \mathbf{e}_{10}(\mathbf{y}) \, dx. \quad (32)$$

We consider uncertainties with respect to the waveguide's geometry and material properties. The corresponding RVs follow uniform distributions centered around the respective nominal values, presented in Table 1. For the geometrical parameters we allow a 10% variation around the nominal

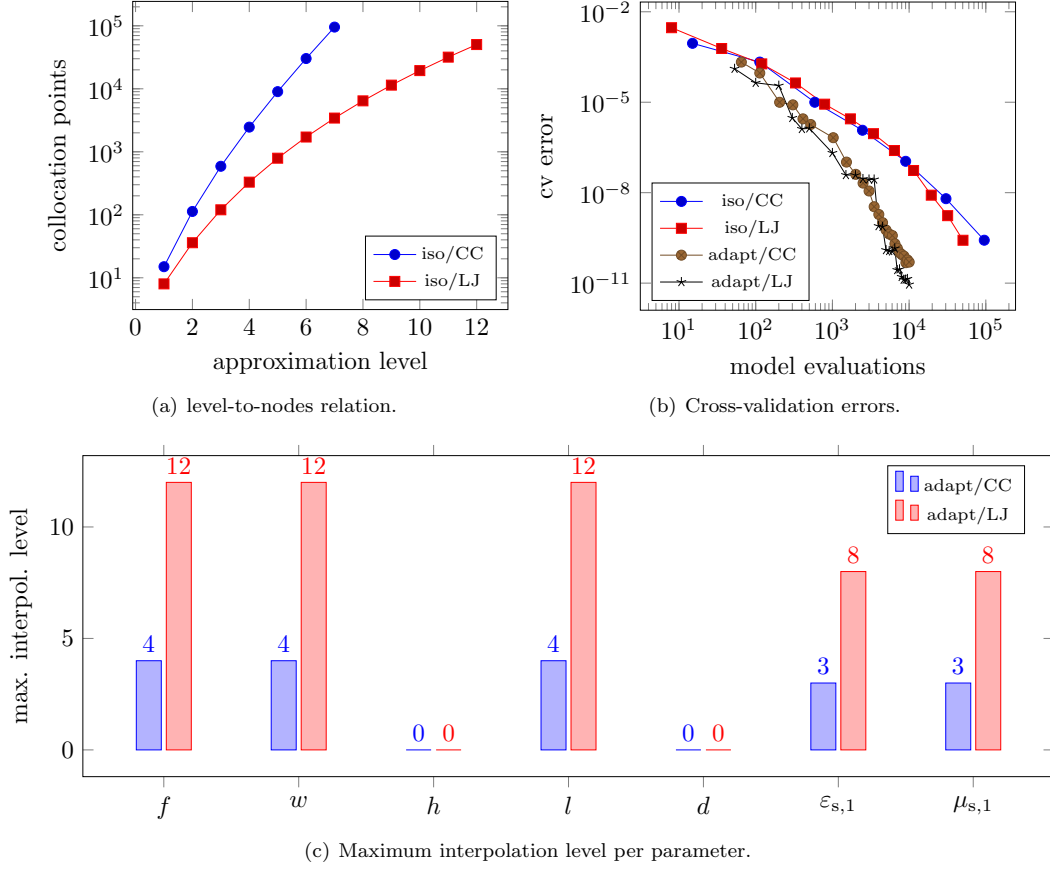


Figure 2: Numerical results for the dielectric slab waveguide with 1st order Debye relaxation and 7 parameters.

value, while an 1% variation is assumed for material parameters. Moreover, the waveguide's operating frequency may take any value in the frequency range $[f_{\min}, f_{\max}]$. Frequency is therefore added to the parameter vector with the assumption that it is uniformly distributed in the frequency range.

Two waveguide models are considered, corresponding to medium- and high-dimensional uncertainty, respectively. The first model employs 1st order Debye relaxation and a total of 7 parameters, namely $f, w, h, l, d, \varepsilon_{s,1}, \mu_{s,1}$. The second model employs 2nd order Debye relaxation and a total of 15 parameters, namely $f, w, h, l, d, \varepsilon_{s,1}, \varepsilon_{s,2}, \varepsilon_{\infty}, \tau_{\varepsilon,1}, \tau_{\varepsilon,2}, \mu_{s,1}, \mu_{s,2}, \mu_{\infty}, \tau_{\mu,1}, \tau_{\mu,2}$.

4.1.2 Numerical results

Results for the 1st waveguide model with 7 parameters are presented in Fig. 2. Results for the 2nd waveguide model with 15 parameters are shown in Fig. 3. For the isotropic cases, Fig. 2(a) and 3(a) show the relation between the approximation level and the required computational work, equivalently number of collocation points. As already discussed in Section 3, each collocation point

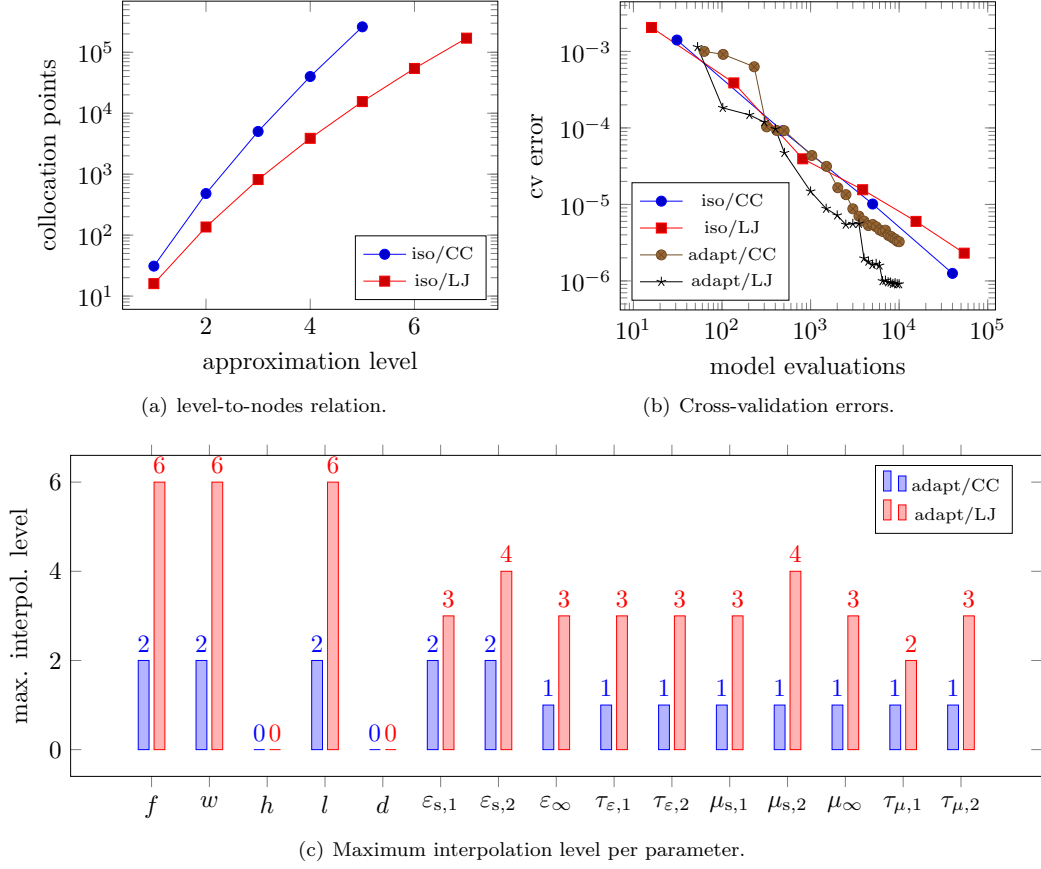


Figure 3: Numerical results for the dielectric slab waveguide with 2nd order Debye relaxation and 15 parameters.

corresponds to a single model evaluation. The curse of dimensionality is particularly evident in Fig. 3(a). Cross-validation error results based on a random sample with $M = 10^4$ entries are shown in Fig. 2(b) and 3(b). For the most accurate adaptive approximations available, we present the maximum interpolation levels per parameter in Fig. 2(c) and 3(c) as an indication to the anisotropy among the input parameters.

In the case of the 1st waveguide model, Leja nodes generally outperform Clenshaw-Curtis for both isotropic and dimension-adaptive collocation. However, the advantage of Leja nodes is not significant. Overall, we may say that both choices of collocation nodes perform comparably well, with Leja nodes having a slight edge. As shown in Fig. 2(c), parameters h and d are completely ignored by the dimension-adaptive algorithm. The most refined parameters are f , w and l , followed by the two material parameters. Due to its level-to-nodes function $m_n(\ell_n) = \ell_n + 1$, the most accurate Leja-based surrogate model employs polynomials of lower degrees than its Clenshaw-Curtis counterpart, where $m_n(\ell_n) = 2^{\ell_n} + 1$.

In the case of the high-dimensional 2nd waveguide model, Clenshaw-Curtis nodes outperform

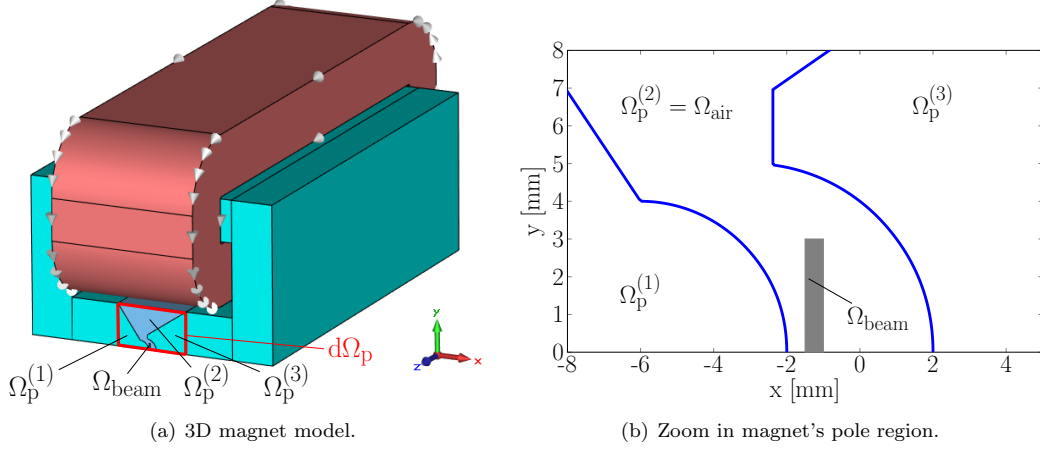


Figure 4: Right: 3D model of one-half of a Rabi-type Stern-Gerlach magnet. Left: Zoom in the magnet's pole region. Modified pictures from [30].

Leja in the case of isotropic sparse grids. The opposite is true for the dimension-adaptive collocation, where Leja nodes perform consistently better than Clenshaw-Curtis. For the most part, the advantage of Leja nodes is significant, particularly for errors below 10^{-5} . As in the case of model 1, parameters h and d are disregarded by the dimension-adaptive algorithm, which again refines parameters f , w and l the most, followed by the material parameters. In this case, the resulting polynomial degrees for both choices of interpolation nodes are comparable.

4.2 Stern-Gerlach Magnet

We consider a real-world application, in particular a Rabi-type Stern-Gerlach magnet (see Fig. 4(a)), similar to the one described in [21] and further studied in [30, 31]. This magnet is currently in use at KU Leuven. Stern-Gerlach magnets are typically employed for the magnetic separation of atom beams or clusters. A key design requirement is a homogeneous magnetic field with a strong gradient. Due to design and manufacturing imperfections, the pole region might suffer from geometrical uncertainties, which in their turn affect the field homogeneity and gradient. The aim of this study is to apply the aforementioned UQ methods in order to quantify the impact of geometrical uncertainties onto the QoI, which is here the average magnetic field gradient in the magnet's beam area.

4.2.1 Model

All computations are performed using a linearized two-dimensional model of the magnet's cross-section, as in [30]. The magnet's pole region, denoted with Ω_p , is the only domain which is spatially resolved. Domain Ω_p is decomposed into distinct patches $\Omega_p^{(i)}$, $i = 1, \dots, 3$, with numbering from left to right, such that $\Omega_p = \Omega_p^{(1)} \cup \Omega_p^{(2)} \cup \Omega_p^{(3)}$. Region $\Omega_p^{(2)}$ refers to the air gap inside the magnet's pole region, while regions $\Omega_p^{(1)}$ and $\Omega_p^{(3)}$ to the regions on the left and right of the air gap, respectively, as in Fig. 4(b). The contributions of the remaining yoke part and the coils are taken into account by a field-circuit coupling and a magnetic equivalent circuit [30]. More precisely, in a first step, the

magnetic vector potential and the magnetic flux through the iron yoke are computed for the entire geometry. The values are denoted as A_z^0 and Φ^0 , respectively. Then, the coupling is realized by imposing

$$A_z = A_\Phi = \Phi / \Phi^0 A_z^0, \quad \text{on } \partial\Omega_p, \quad (33)$$

where Φ is recomputed for a different geometry using magnetic circuit theory. Let I and N_c represent the coil current and the number of turns in the winding, respectively. Then this relation can be abstractly written as $F(A_z, \Phi) = N_c I$, where F refers to the magnetomotive force. For details, the reader is referred to [30]. In summary, the field-circuit coupled problem reads

$$\text{div}(\nu \text{grad} A_z) = 0, \quad \text{in } \Omega_p, \quad (34a)$$

$$A_z - A_\Phi = 0, \quad \text{on } \partial\Omega_p, \quad (34b)$$

$$F(A_z, \Phi) = N_c I, \quad (34c)$$

where ν refers to the magnetic reluctivity. The magnetic flux density \vec{B} is obtained as $\vec{B} = (\partial_y A_z, -\partial_x A_z, 0)$. The magnet's beam area is denoted with Ω_{beam} and lies inside the air gap of the pole region, denoted with Ω_{air} , where $\Omega_{\text{air}} = \Omega_p^{(2)}$ (see Fig. 4(b)). Denoting with $\tau(x, y) = \frac{\partial |\vec{B}|}{\partial x}$ the magnetic field gradient in the x -direction, the average field gradient in the beam area is given by

$$q = \tau_{\text{avg}} = \frac{1}{|\Omega_{\text{beam}}|} \int_{\Omega_{\text{beam}}} \tau(x, y) d\Omega. \quad (35)$$

Isogeometric analysis (IGA) is employed for the spatial discretization [16]. In IGA, both the solution variable A_z and the geometry are described in terms of non-uniform rational B-splines (NURBS). A generic NURBS curve reads

$$\vec{R}(\xi) = \sum_{i=1}^N \vec{P}_i N_i^p(\xi), \quad \xi \in [0, 1], \quad (36)$$

where \vec{P}_i and N_i^p refer to a control point and a NURBS basis function of degree p , respectively. NURBS basis functions are defined as

$$N_i^p(\xi) = \frac{w_i B_i^p(\xi)}{\sum_{j=1}^N w_j B_j^p(\xi)}, \quad (37)$$

with weights w_i and B-spline basis functions B_i^p , respectively.

The original NURBS curves defining the three patches $\Omega_p^{(i)}$, $i = 1, 2, 3$, are depicted in Fig. 5 in blue, while a geometry variation is given in red. We introduce random geometry deformations by regarding the control points and weights of these curves as uncertain. More precisely, we introduce 10 RVs corresponding to the x and y coordinates of 4 control points and 2 weights, as presented in Table 2. Then, we obtain a random reluctivity as

$$\nu(\mathbf{y}) = \nu_{\text{iron}} \mathbb{1}_{\Omega_p^{(1)}(\mathbf{y})} + \nu_{\text{air}} \mathbb{1}_{\Omega_p^{(2)}(\mathbf{y})} + \nu_{\text{iron}} \mathbb{1}_{\Omega_p^{(3)}(\mathbf{y})}, \quad (38)$$

with $\mathbb{1}_{\Omega_p^{(i)}}$ denoting the characteristic function of patch i and ν_{iron} and ν_{air} denoting the reluctivity of iron and air, respectively. Accordingly, the parametric field-circuit coupled problem reads

$$\text{div}(\nu(\mathbf{y}) \text{grad} A_z) = 0, \quad \text{in } \Omega_p, \quad (39a)$$

$$A_z - A_\Phi = 0, \quad \text{on } \partial\Omega_p, \quad (39b)$$

$$F(A_z, \Phi) = N_c I, \quad (39c)$$

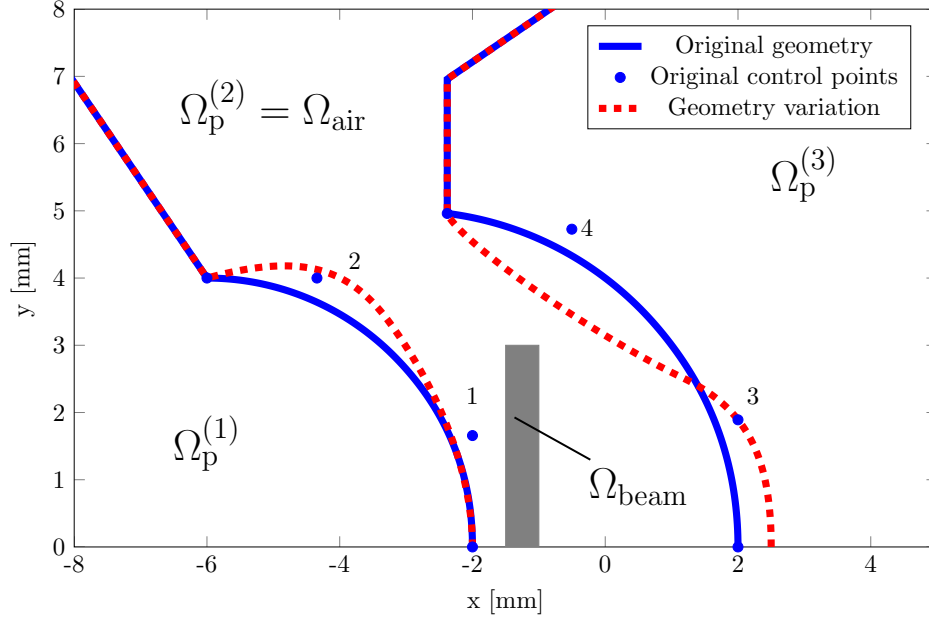


Figure 5: Original and varied geometry of the magnet's pole region. Modified picture from [30].

with ρ_Y -almost everywhere in Γ . Assuming that problem (39) is well-posed, the quantity of interest is itself a random variable.

Table 2: Control point uncertainties and uniform distribution limits.

Parameter	Bottom Limit	Upper Limit	Units
x_1	-3.00	-2.00	[mm]
y_1	1.66	2.0	[mm]
x_2	-5.0	-2.0	[mm]
y_2	2.50	4.50	[mm]
w_2	0.35	2.85	[-]
x_3	1.50	2.50	[mm]
y_3	1.89	2.5	[mm]
x_4	-2.0	2.0	[mm]
y_4	4.0	5.50	[mm]
w_4	0.37	2.87	[-]

4.2.2 Numerical results

All results are presented in Fig. 6. Fig. 6(a) shows the relation between approximation level and number of collocation points of the isotropic sparse grids for the case of 10 parameters. The Stern-Gerlach magnet simulation is based on an expensive numerical model, therefore approximation levels $\ell = 5$ for the Clenshaw-Curtis case and or $\ell = 7$ for the Leja case already result in hampering

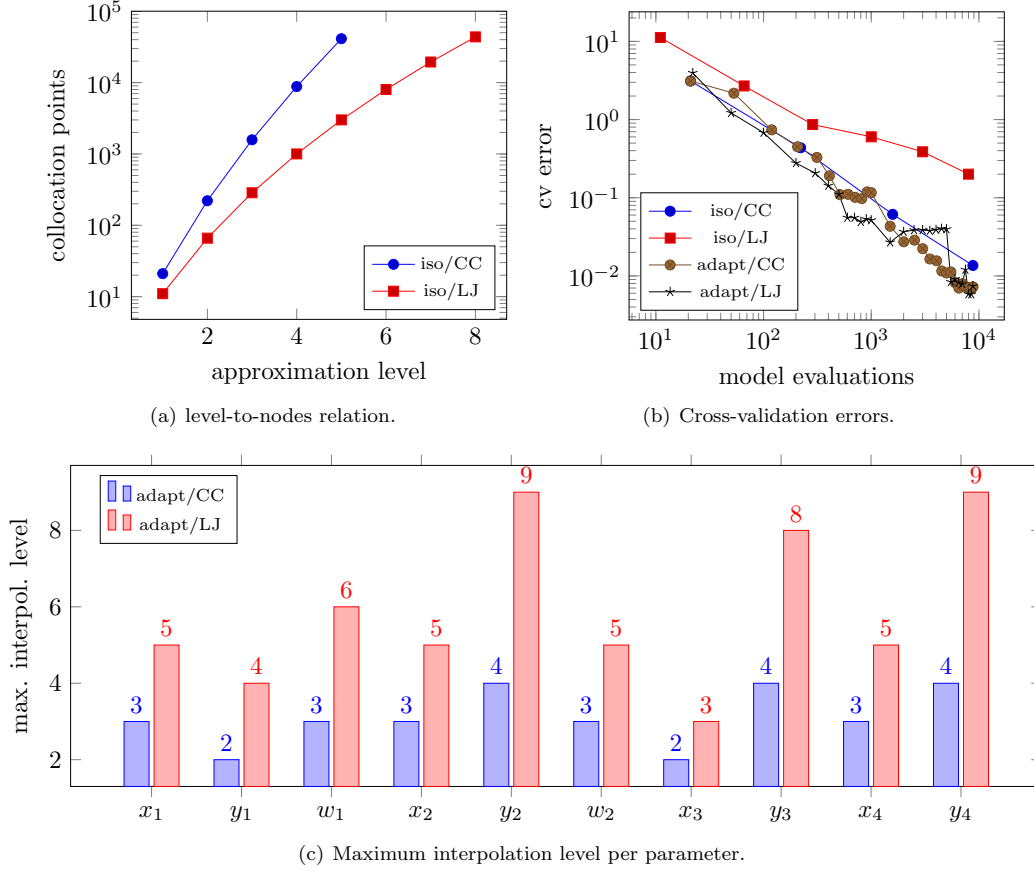


Figure 6: Numerical results for the Stern-Gerlach magnet with 10 parameters.

computational costs. Because of the high computational cost of the magnet model, cross-validation errors are now computed using a sample with $M = 10^3$ entries. Error results are presented in Fig. 6(b). Maximum interpolation levels per parameter for the most accurate approximations are shown in Fig. 6(c).

We observe that isotropic Clenshaw-Curtis collocation outperforms significantly its Leja-based counterpart. Both dimension-adaptive schemes outperform isotropic collocation. In this case, computational gains are not as pronounced as in the waveguide example. This could be attributed to the considered QoI and possible difficulties in its approximation. Another possible explanation could be that strong anisotropy among the parameters is not present in this problem. This explanation is supported by the results presented in Fig. 6(c) for the Clenshaw-Curtis case, where all parameters are refined with levels either 3 or 4. Stronger parameter anisotropy can be observed in the Leja case, however this can be attributed to the more granular level-to-nodes function of Leja nodes. It is possible that the approximation levels become comparable as the approximation accuracy increases. In general, the dimension-adaptive algorithm seems to perform similarly for both choices of interpolation nodes. For the most part, Leja nodes have a small advantage over Clenshaw-Curtis,

however both families of interpolation nodes perform comparably. The algorithm seems to recognize deformations in the y -direction as more important than deformations in the x -direction, hence coordinates y_2 , y_3 and y_4 are refined more than all other parameters. For all parameters, polynomials employed in the Clenshaw-Curtis approximation are of significantly higher orders than in the Leja case.

5 Summary and Conclusions

We have investigated the performance of the sparse grids stochastic collocation method, when used for the construction of accurate polynomial surrogates of computational EMF models. Two models suffering from medium- to high-dimensional input uncertainty have been used for that purpose. We have employed both isotropic and adaptively constructed, anisotropic sparse grids based on Clenshaw-Curtis and Leja interpolation nodes, under the assumption that all input parameters are statistically independent and uniformly distributed. In all examples, dimension-adaptive collocation outperforms the isotropic variant. In cases characterized by strong parameter anisotropy, the computational gains are even impressive. In all examples, Leja-based dimension-adaptive collocation either has an advantage over its Clenshaw-Curtis-based counterpart with respect to surrogate model accuracy as measured with the cross-validation error metric, or performs comparably well. These findings are in agreement with the available literature results, see e.g. [26]. Follow-up studies based on the present work should consider the use of sufficiently accurate surrogate models for computationally demanding tasks, e.g. surrogate-based robust optimization or failure probability estimations. Moreover, while the use of Leja nodes in UQ problems with non-uniformly distributed parameters is suggested in [26], the authors provide numerical examples only for the uniform and Gaussian case. Therefore, the use of Leja points with different probability distributions should be further explored.

Acknowledgments

All authors would like to thank our colleague Andreas Pels for providing the Stern-Gerlach magnet model. The first and third author would like to acknowledge the support of the Graduate School of Computational Engineering, Technische Universität Darmstadt.

References

- [1] I. BABUSKA, F. NOBILE, AND R. TEMPONE, *A Stochastic Collocation Method for Elliptic Partial Differential Equations with Random Input Data*, SIAM Review, (2010), pp. 317–355.
- [2] I. BABUSKA, R. TEMPONE, AND G. E. ZOURARIS, *Galerkin Finite Element Approximations of Stochastic Elliptic Partial Differential Equations*, SIAM J. Numerical Analysis, 42 (2004), pp. 800–825.
- [3] V. BARTHELMANN, E. NOVAK, AND K. RITTER, *High Dimensional Polynomial Interpolation on Sparse Grids*, Adv. Comput. Math., 12 (2000), pp. 273–288.
- [4] D. BELLMAN, *Dynamic Programming*, Princeton University Press, 1957.
- [5] G. BLATMAN AND B. SUDRET, *Adaptive Sparse Polynomial Chaos Expansion Based on Least Angle Regression*, J. Comput. Physics, 230 (2011), pp. 2345–2367.

- [6] H.-J. BUNGARTZ AND M. GRIEBEL, *Sparse Grids*, Acta Numerica, 13 (2004), pp. 147–269.
- [7] A. CHKIFA, A. COHEN, AND C. SCHWAB, *High-Dimensional Adaptive Sparse Polynomial Interpolation and Applications to Parametric PDEs*, Foundations of Computational Mathematics, 14 (2014), pp. 601–633.
- [8] P. G. CONSTANTINE, *Active Subspaces: Emerging Ideas for Dimension Reduction in Parameter Studies*, Society for Industrial and Applied Mathematics, Philadelphia, PA, USA, 2015.
- [9] M. S. ELDRED, *Comparison of Non-Intrusive Polynomial Chaos and Stochastic Collocation Methods for Uncertainty Quantification*, In: AIAA, (2009).
- [10] J. FEINBERG AND H. P. LANGTANGEN, *Chaospy: An Open Source Tool for Designing Methods of Uncertainty Quantification*, J. Comput. Science, 11 (2015), pp. 46–57.
- [11] T. GERSTNER AND M. GRIEBEL, *Dimension-Adaptive Tensor-Product Quadrature*, Computing, 71 (2003), pp. 65–87.
- [12] R. G. GHANEM AND P. D. SPANOS, *Stochastic Finite Elements: A Spectral Approach*, Springer-Verlag New York, Inc., New York, NY, USA, 1991.
- [13] L. GIRALDI, A. LITVINENKO, D. LIU, H. G. MATTHIES, AND A. NOUY, *To Be or Not to Be Intrusive? The Solution of Parametric and Stochastic Equations - the "Plain Vanilla" Galerkin Case*, SIAM J. Scientific Computing, 36 (2014).
- [14] M. GRIEBEL, *Adaptive Sparse Grid Multilevel Methods for Elliptic PDEs Based on Finite Differences*, Computing, 61 (1998), pp. 151–180.
- [15] W. HACKBUSCH, *Numerical Tensor Calculus*, Acta Numerica, 23 (2014), p. 651–742.
- [16] T. J. HUGHES, J. A. COTTRELL, AND Y. BAZILEVS, *Isogeometric Analysis: CAD, Finite Elements, NURBS, Exact Geometry and Mesh Refinement*, Computer methods in applied mechanics and engineering, 194 (2005), pp. 4135–4195.
- [17] J. D. JAKEMAN AND T. WILDEY, *Enhancing Adaptive Sparse Grid Approximations and Improving Refinement Strategies Using Adjoint-Based A Posteriori Error Estimates*, J. Comput. Physics, 280 (2015), pp. 54–71.
- [18] J.-M. JIN, *The Finite Element Method in Electromagnetics*, John Wiley & Sons, 2015.
- [19] A. KLIMKE, *Sparse Grid Interpolation Toolbox – User’s Guide*, Tech. Rep. IANS 2007/017, University of Stuttgart, 2007.
- [20] A. KLIMKE AND B. I. WOHLMUTH, *Algorithm 847: Spinterp: Piecewise Multilinear Hierarchical Sparse Grid Interpolation in MATLAB*, ACM Trans. Math. Softw., 31 (2005), pp. 561–579.
- [21] B. MASSCHAELE, T. ROGGEN, H. DE GERSEM, E. JANSSENS, AND T. T. NGUYEN, *Design of a Strong Gradient Magnet for the Deflection of Nanoclusters*, IEEE Transactions on Applied Superconductivity, 22 (2012).
- [22] H. G. MATTHIES AND A. KEESE, *Galerkin Methods for Linear and Nonlinear Elliptic Stochastic Partial Differential Equations*, Informatik-Berichte der Technischen Universität Braunschweig, 2003-08.

- [23] G. MIGLIORATI, *Adaptive Polynomial Approximation by Means of Random Discrete Least Squares*, in ENUMATH, A. Abdulle, S. Deparis, D. Kressner, F. Nobile, and M. Picasso, eds., vol. 103 of Lecture Notes in Computational Science and Engineering, Springer, 2013, pp. 547–554.
- [24] G. MIGLIORATI, F. NOBILE, E. VON SCHWERIN, AND R. TEMPONE, *Approximation of Quantities of Interest in Stochastic PDEs by the Random Discrete L_2 Projection on Polynomial Spaces*, SIAM J. Scientific Computing, 35 (2013).
- [25] ———, *Analysis of Discrete L_2 Projection on Polynomial Spaces with Random Evaluations*, Foundations of Computational Mathematics, 14 (2014), pp. 419–456.
- [26] A. NARAYAN AND J. D. JAKEMAN, *Adaptive Leja Sparse Grid Constructions for Stochastic Collocation and High-Dimensional Approximation*, SIAM J. Scientific Computing, 36 (2014).
- [27] F. NOBILE, L. TAMELLINI, AND R. TEMPONE, *Comparison of Clenshaw–Curtis and Leja Quasi-Optimal Sparse Grids for the Approximation of Random PDEs*, Springer International Publishing, Cham, 2015, pp. 475–482.
- [28] F. NOBILE, R. TEMPONE, AND C. G. WEBSTER, *A Sparse Grid Stochastic Collocation Method for Partial Differential Equations with Random Input Data*, SIAM J. Numerical Analysis, 46 (2008), pp. 2309–2345.
- [29] ———, *An Anisotropic Sparse Grid Stochastic Collocation Method for Partial Differential Equations with Random Input Data*, SIAM J. Numerical Analysis, 46 (2008), pp. 2411–2442.
- [30] A. PELS, Z. BONTINCK, J. CORNO, H. DE GERSEM, AND S. SCHÖPS, *Optimization of a Stern-Gerlach Magnet by Magnetic Field-Circuit Coupling and Isogeometric Analysis*, IEEE Transactions on Magnetics, 51 (2015).
- [31] U. RÖMER, S. SCHÖPS, AND H. DE GERSEM, *A Defect Corrected Finite Element Approach for the Accurate Evaluation of Magnetic Fields on Unstructured Grids*, J. Comput. Physics, 335 (2017), pp. 688–699.
- [32] B. SCHIECHE, *Unsteady Adaptive Stochastic Collocation on Sparse Grids*, PhD Thesis, TU Darmstadt, 2012.
- [33] S. A. SMOLYAK, *Quadrature and Interpolation Formulas for Tensor Products of Certain Classes of Functions*, Dokl. Acad. Nauk SSSR, 4 (1963), pp. 240–243.
- [34] L. TAMELLINI AND F. NOBILE, *Sparse Grids MATLAB Kit*. URL: <http://csqi.epfl.ch>. Accessed: 15.08.2017.
- [35] D. XIU AND J. S. HESTHAVEN, *High-Order Collocation Methods for Differential Equations with Random Inputs*, SIAM J. Scientific Computing, 27 (2005), pp. 1118–1139.
- [36] D. XIU AND G. E. KARNIAKAKIS, *The Wiener-Askey Polynomial Chaos for Stochastic Differential Equations*, SIAM J. Scientific Computing, 24 (2002), pp. 619–644.